energies

MDPI

Article

Effect of Microwave Processing and Glass Inclusions on Thermoelectric Properties of P-Type Bismuth Antimony Telluride Alloys for Wearable Applications

Amin Nozariasbmarz [1,2] and Daryoosh Vashaee [1,2,*]

[1] Electrical and Computer Engineering Department, Monteith Research Center, North Carolina State University, Raleigh, NC 27606, USA; anozari@ncsu.edu

[2] Materials Science and Engineering Department, Monteith Research Center, North Carolina State University, Raleigh, NC 27606, USA

* Correspondence: dvashae@ncsu.edu; Tel.: +1-(919)-515-9599

Received: 28 July 2020; Accepted: 25 August 2020; Published: 1 September 2020

Abstract: Depending on the application of bismuth telluride thermoelectric materials in cooling, waste heat recovery, or wearable electronics, their material properties, and geometrical dimensions should be designed to optimize their performance. Recently, thermoelectric materials have gained a lot of interest in wearable electronic devices for body heat harvesting and cooling purposes. For efficient wearable electronic devices, thermoelectric materials with optimum properties, i.e., low thermal conductivity, high Seebeck coefficient, and high thermoelectric figure-of-merit (zT) at room temperature, are demanded. In this paper, we investigate the effect of glass inclusion, microwave processing, and annealing on the synthesis of high-performance p-type $(Bi_xSb_{1-x})_2Te_3$ nanocomposites, optimized specially for body heat harvesting and body cooling applications. Our results show that glass inclusion could enhance the room temperature Seebeck coefficient by more than 10% while maintaining zT the same. Moreover, the combination of microwave radiation and post-annealing enables a 25% enhancement of zT at room temperature. A thermoelectric generator wristband, made of the developed materials, generates 300 μW power and 323 mV voltage when connected to the human body. Consequently, MW processing provides a new and effective way of synthesizing p-type $(Bi_xSb_{1-x})_2Te_3$ alloys with optimum transport properties.

Keywords: thermoelectric materials; microwave processing; bismuth telluride; nanocomposites; body heat harvesting; glass inclusion; annealing; wearable cooler

1. Introduction

Thermoelectric (TE) materials are able to generate electricity from a temperature gradient directly. The quality of these materials is defined by dimensionless thermoelectric figure of merit (zT) which is defined by $zT = (S^2\sigma/\kappa)T$, where S, σ, κ and T are the Seebeck coefficient (thermopower), electrical conductivity, thermal conductivity, and absolute temperature, respectively. $S^2\sigma$ is known as the TE power factor (PF) [1]. Bismuth antimony telluride (BiSbTe) alloys are the most promising p-type TE materials that are widely used for cooling and low-temperature power generation applications. BiSbTe alloys have been extensively developed in the last two decades [2–6]. In 2008, a nanostructured BiSbTe bulk alloy was synthesized via mechanical alloying and showed zT = 1.4 at 100 °C [2]. Afterward, various studies showed enhanced TE properties in BiSbTe alloys through different synthesis methods via the reduction of thermal conductivity and/or power factor enhancement [3–7].

Nanocomposites are designated to a broad class of materials; however, in thermoelectrics, they are generally considered as materials that contain nano-grains or nano-features as the second phase in their

matrix. It has been shown that nanocomposites can have lower thermal conductivity than the "alloy limit" [8]. zT improvement has been achieved in several TE nanocomposites such as PbTe-SrTe [9], InGaAs/ErAs [8,10], SiGe-$FeSi_2$ [11], and SiGe-Mg_2Si [12,13]. TE nanocomposites undergo different electrical and thermal transport processes than other TE materials such as dopant precipitation, reduction in bipolar effect, and scattering of phonons at interfaces that can improve the TE properties in nanocomposites [14]. Hence, depending on the application of TE materials, defect engineering, grain size refinement, and compositional optimization enable further optimization of TE properties.

Using TE materials in wearable electronics to harvest energy from body heat is an emerging technique to replace rechargeable batteries [15]. For wearable power generators and coolers, materials with high zT and low thermal conductivity are demanded due to the skin and heatsink thermal resistance and practical constraints restricting the use of bulky heatsinks. [16,17]. In addition, a high Seebeck coefficient is required to provide adequate voltage to run the power management unit [18]. Therefore, for the wearable platform, the TE properties of materials should be optimized to perform most efficiently at room temperature.

The reduction of thermal conductivity by phonon scattering in bulk TE materials has been widely studied [2–5]. Most of the reported low thermal conductivity in BiSbTe alloys are from bottom-up methods that usually have higher control on the microstructure [5,19,20]. However, these methods are slow and costly. Microwave (MW) processing [21–23] is a reliable top-down technique that has great potential to generate unique microstructures and improve the TE properties. However, there are only limited studies on the fabrication of TE materials using MW processing [24–30]. In this paper, we introduce MW processing as a new and promising top-down technique for developing efficient p-type $(Bi_xSb_{1-x})_2Te_3$ nanocomposites for wearable applications. The effect of glass inclusions and annealing on the Seebeck coefficient, thermal conductivity, and zT is also studied to design p-type $(Bi_xSb_{1-x})_2Te_3$ nanocomposites for a wearable application.

2. Experimental Procedure

High purity bismuth (Bi, 99.9%) powder/tellurium (Te, 99.9%) lump and antimony (Sb, 99.9%) powder/tellurium (Te, 99.9%) lump were separately mixed according to the stoichiometric ratio and melted in an induction furnace to synthesis uniform Bi_2Te_3 and Sb_2Te_3 ingots (Figure 1a,b). In order to tune for probable tellurium loss during the melting process, 2% extra Te was added to the mixture of Bi/Te and Sb/Te. The synthesized ingots were then pulverized and milled for 5 h using a Fritsch-P6 planetary ball mill to prepare uniform nanostructured powders (Figure 1c). Bi_2Te_3 and Sb_2Te_3 powders were then weighted and mixed with different ratios. In order to study the effect of glass frit, different types and amount of glass powders, including EG3021, EG2964, EG2782, EG0026 Ferro electronic glass [31,32] as sintering aids were added to the mixture of Bi_2Te_3/Sb_2Te_3 powders and all of the powders were separately mixed for 30 s in an ARE-310 Thinky mixer to make $(Bi_xSb_{1-x})_2Te_3$ nanocomposites. The powders were then sintered at 540 °C for one minute using spark plasma sintering (SPS) to fabricate TE samples with 14 mm height and 6 mm diameter.

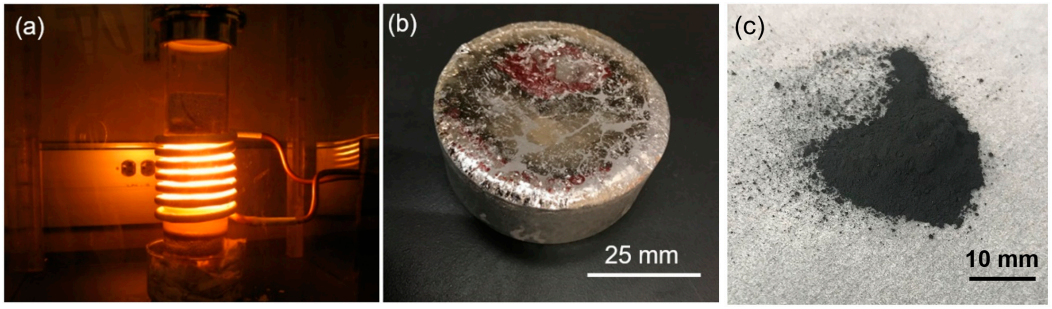

Figure 1. (**a**) Induction melting process, (**b**) a synthesized Bi_2Te_3 ingot made from induction melting, and (**c**) the uniform powder after ball milling.

In order to study the effect of MW processing, the samples were exposed to MW radiation inside a single-mode cavity using a 2.45 GHz MW generator. The experimental MW system comprises an E-H tuner to adjust the magnitude of the wave and a sliding short for continuous load matching during the processing. A pyrometer detector is used to observe the temperature profile of the samples. All the preparation steps are performed under an argon atmosphere. The samples are loaded into a boron nitride crucible and then hermetically sealed inside a quartz tube. The quartz tube is then deoxidized by vacuum and Ar purge multiple times. The pressure of argon inside the tube is maintained at 700 torrs during the experiments. The samples are processed by MW radiation at ~500 °C. Due to the reduction of the density of the MW-processed samples, they were further consolidated by SPS at 400 °C to densify and improve their mechanical properties. The annealing was performed in an atmosphere-controlled oven at 230 °C.

The phase identification of the samples was performed by X-ray diffraction (XRD) using a PANalytical Empyrean with Cu-K_α radiation. The morphology and microstructure of the samples were investigated by a field emission scanning electron microscope (FE-SEM) using an FEI Verios 460L. The electrical resistivity and Seebeck coefficient of the samples were simultaneously measured using a 4-probe Ulvac ZEM-3 instrument. The thermal conductivity (κ) of the samples was calculated by $\kappa = D\rho C_p$, where thermal diffusivity (D) of the samples was measured using a Netzsch's LFA 457 Micro Flash laser flash instrument, the density (ρ) of the samples was measured using the Archimedes' method, and the specific heat capacity (C_p) was measured by Simultaneous Thermal Analyzer (STA, Netzsch 449 F1 Jupiter) instrument.

3. Results and Discussion

TE properties and leg dimensions of $(Bi_xSb_{1-x})_2Te_3$ alloys should be optimized depending on their specific applications [33]. For example, for wearable applications, high aspect ratio (thin and tall) legs with a large Seebeck coefficient, small thermal conductivity, and high zT at room temperature are demanded [19,34]. However, one of the drawbacks of thin and tall $(Bi_xSb_{1-x})_2Te_3$ legs is their poor mechanical properties versus shear and compressive forces that limit the cross-section reduction of the legs. It has been shown that Ferro electronic glasses can improve the mechanical properties of TE materials while improving or maintaining TE properties [24,35]. The effect of the addition of different glass inclusions on thermoelectric properties of $(Bi_xSb_{1-x})_2Te_3$ is studied in the next section.

3.1. Effect of Glass Inclusion

Ferro electronic glasses are used as a sintering aid in ceramics, binding agents, and sealants [36]. Table 1 summarizes compositions, glass transition temperature (T_g), softening temperature, and density of different glasses that are used in this study. Different Ferro glasses can have very different effects on the TE properties of $(Bi_xSb_{1-x})_2Te_3$ alloys. Figure 2 compares the effect of the addition of 5 wt% EG3021, EG2964, EG2782, and EG0026 glasses on the TE properties of $(Bi_{0.25}Sb_{0.75})_2Te_3$. EG3021 severely deteriorated the TE properties of the alloy, specifically its electrical conductivity in all temperature ranges. Only the room temperature Seebeck coefficient enhances to ~270 μV/K. This might be due to the low T_g and softening temperature of EG3021 or the glass elements that probably has a destructive effect on carrier transport. Among EG2964, EG2782, and EG0026 glasses, EG2964 provides better TE properties than the others up to 100 °C by improving the Seebeck coefficient and reducing the thermal conductivity. It results in the lowest thermal conductivity (=0.73 W/mK) and the highest zT (=0.9) at room temperature. The softening point of EG2964 is 520 °C, which almost matches with the SPS temperature of the $(Bi_{0.25}Sb_{0.75})_2Te_3$ alloy, i.e., 540 °C. Compared to the other glasses, the addition of EG2964 glass (i.e., a composition made of Bi, Zn, and B) can be positively attributed to the transport properties of $(Bi_{0.25}Sb_{0.75})_2Te_3$ alloy by optimizing dopant level and the reduction of lattice thermal conductivity.

Table 1. Properties of different Ferro glasses.

Glass	Composition	T_g (°C)	Softening Temp (°C)	Density (g/cm^3)
EG3021	Bi-Zn-B-R2O	365	383	7.06
EG2964	Bi-Zn-B	480	520	4.00
EG2782	Si-B-Al-RO	640	745	2.56
EG0026	Al-Ca-B-Si	641	770	2.60

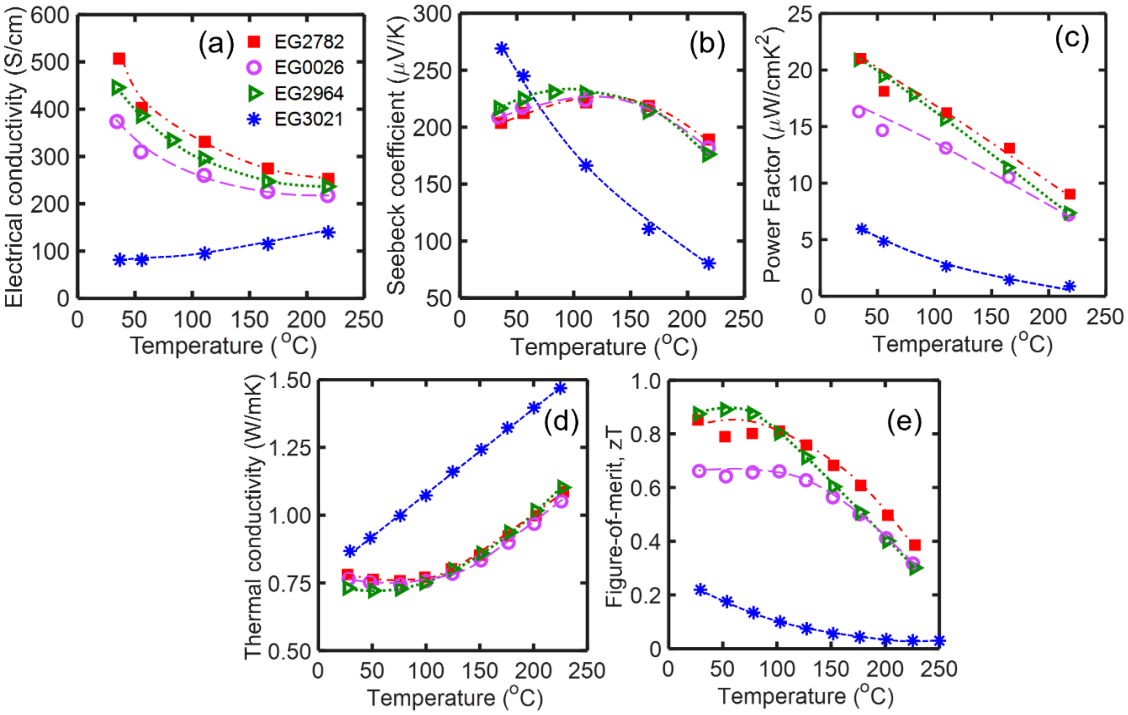

Figure 2. Comparison of (**a**) electrical conductivity, (**b**) Seebeck coefficient, (**c**) thermoelectric (TE) power factor (PF), (**d**) thermal conductivity, and (**e**) TE figure-of-merit (zT) of $(Bi_{0.25}Sb_{0.75})_2Te_3$ alloys including 5 wt% EG3021, EG2964, EG2782, and EG0026 glass inclusions.

3.2. Optimization of Glass Inclusions

As was mentioned earlier, EG2964 glass inclusion provides better TE properties than other types of glasses. In order to optimize the amount of glass inclusions in $(Bi_xSb_{1-x})_2Te_3$ alloys, 0, 2.5, 5, and 7.5 wt% of EG2964 glass were added to the mixture of $(Bi_{0.25}Sb_{0.75})_2Te_3$. Figure 3 compares TE properties of samples with glass inclusions. In general, the addition of more glass inclusions reduces the electrical conductivity and improves the Seebeck coefficient. Above 100 °C the increase in thermal conductivity and the reduction of the Seebeck coefficient are both the result of bipolar diffusion when the concentration of the minority carriers becomes comparable to those of the majority ones. The addition of glass does not change the trend of TE properties; it only shifts the bipolar effect to lower temperature. The sample without glass has the lowest Seebeck coefficient at room temperature. The PF of the sample with 5 wt% EG2964 is the highest among all samples, and the addition of more than 5% glass results in the reduction of PF. The sample without glass has the lowest thermal conductivity, and the addition of glass increases the thermal conductivity of $(Bi_{0.25}Sb_{0.75})_2Te_3$ alloy. The addition of 5% EG2964 glass has the lowest deteriorating effect on room temperature zT of $(Bi_xSb_{1-x})_2Te_3$ alloys while it improves the Seebeck coefficient and mechanical properties.

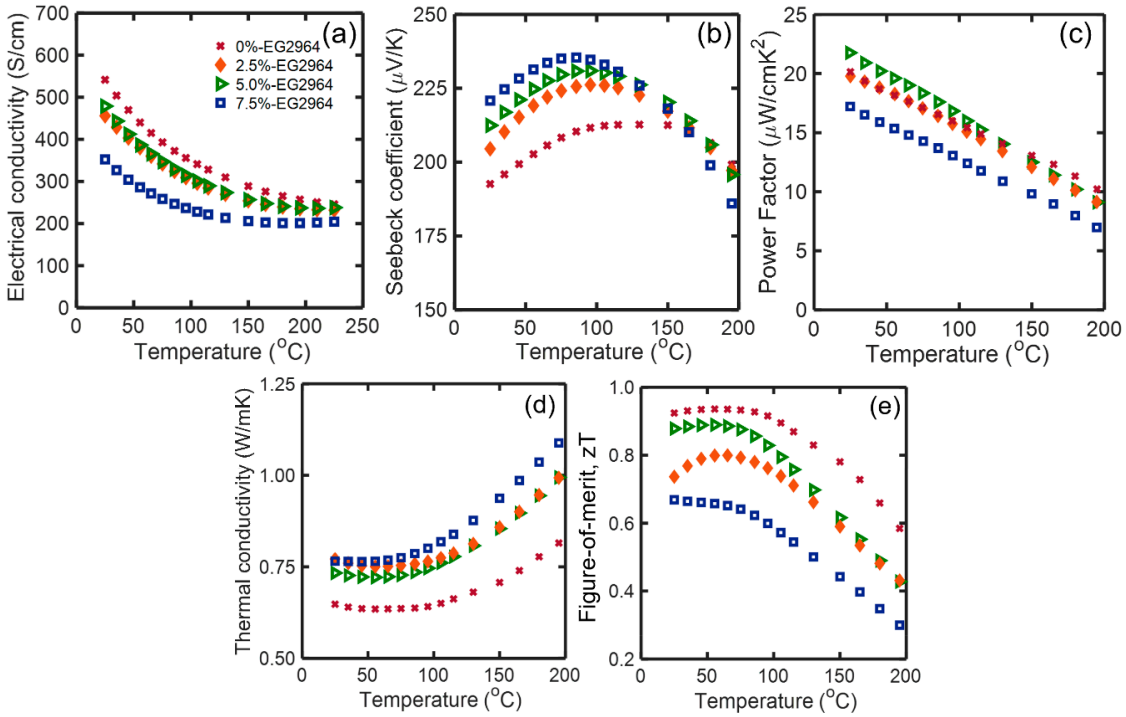

Figure 3. Effect of 0, 2.5, 5 and 7.5 wt% of EG2964 glass on (**a**) electrical conductivity, (**b**) Seebeck coefficient, (**c**) PF, (**d**) thermal conductivity and, (**e**) zT of $(Bi_{0.25}Sb_{0.75})_2Te_3$.

According to these results, it is expected that in highly doped $(Bi_xSb_{1-x})_2Te_3$ alloys with lower x values wherein the electrical and thermal conductivity are naturally high, the addition of glass reduces the electrical and thermal conductivity while improving the Seebeck coefficient. Therefore, in the next section, we use 5% EG2964 glass and study the effect of MW processing and the consequent annealing to optimize the TE properties of $(Bi_xSb_{1-x})_2Te_3$ with lower x values.

3.3. Microwave Processing of Bismuth Antimony Telluride

MW radiation as an electromagnetic wave interacts with the materials at the atomic level and can cause driving forces to enhance the solid-state reaction [25,26,37]. As such, it offers an efficiently practical way for the synthesis and processing of TE materials. The interaction of MW radiation with materials is divided into thermal and non-thermal effects [25]. The thermal effect has similar basics and consequences as conventional heating. However, the non-thermal effects of MW radiation enable some effects that cannot be explained by equilibrium thermodynamics. Some examples are solid-state reaction, the electromagnetic field induced decrystallization, and solid-solution decomposition of alloys, all of which can be of particular interest for designing efficient TE structures. MW interaction with solid-solution alloys can drive a decomposition process as a result of a strong ponderomotive force (PMF) near the interfaces [38]. The PMF enhances the mass transport near the interfaces (such as grain boundaries) and results in constitutional phase separation. Hence, it enables the fabrication of nanocomposites such as $(Bi_xSb_{1-x})_2Te_3$ with Bi_2Te_3-rich and Sb_2Te_3-rich domains. Electrons and phonons in such nanocomposites experience spectral energy disruption at the interface of two phases that can increase the thermopower and decrease the thermal conductivity, both of which can lead to better TE properties [24,26].

In MW processing of TE materials, the temperature of the samples enhances either by increasing the MW power or increasing the MW exposure time. MW radiation up to a certain temperature, ~500 °C, results in decrystallization and defect generation [39] and/or decomposition [38] of $(Bi_xSb_{1-x})_2Te_3$ alloys. Additives such as sintering aids can also change the response of $(Bi_xSb_{1-x})_2Te_3$ alloys to MW as well as changing their TE properties.

MW processing of p-type $(Bi_xSb_{1-x})_2Te_3$ alloys above 400 °C without applying an external force on the sample results in a dimensional expansion of the SPS sample, which reduces the density of the TE materials. The reason for the expansion is not clearly known yet; however, it is expected that the interaction of MW with the $(Bi_xSb_{1-x})_2Te_3$ alloy results in localized hot spots and tellurium evaporation, which may lead to structural expansion. Hence, a post-SPS at low temperature is required to densify the MW-processed samples.

Annealing is a practical method to optimize the electrical conductivity. However, it can also affect thermal conductivity. In order to investigate the effect of annealing on thermal transport of MW-processed $(Bi_xSb_{1-x})_2Te_3$-5% glass nanocomposites, a sample was diced into five disks with 1 mm thickness and the thermal conductivity of each disk was measured separately. The variation of the thermal conductivity of the disks is shown with error bars in Figure 4a. Then, the disks were annealed at 230 °C in an oven for 0 to 72 h (inset of Figure 4b). The thermal conductivity of $(Bi_xSb_{1-x})_2Te_3$-5% glass decreases up to 40 h of annealing; then, it increases (Figure 4a,b). The lowest thermal conductivity was achieved in the 40 h annealed sample, which might be due to the creation of a composite structure by precipitation and growth of the Bi_2Te_3-rich phase as a second phase in the microstructure. Figure 5 demonstrates the comparison of the XRD patterns of annealed samples at 230 °C for 0, 40, and 70 h. Comparison of 0 h and 40 h annealing shows that although annealing for 40 h results in grain growth (indicated by the narrowing of the XRD peaks), the intensity of Bi_2Te_3 peak at $2\theta = 27.7°$ increases. Therefore, it results in the creation of a composite structure. As mentioned earlier, MW processing can decompose $(Bi_xSb_{1-x})_2Te_3$ alloys to Bi_2Te_3-rich and Sb_2Te_3-rich phases and generate a composite structure [38]. Annealing helps the growth of the decomposed phase, i.e., Bi_2Te_3-rich phase up to a certain point. Longer annealing time at 230 °C leads to the dissolution of the Bi_2Te_3-rich phase in the Sb_2Te_3-rich matrix. According to the XRD pattern, dissolving happens by merging the peaks of the two phases together. This results in thermal conductivity enhancement after 40 h of annealing. Therefore, 40 h annealing at 230 °C is the optimum annealing condition for glass-contained samples.

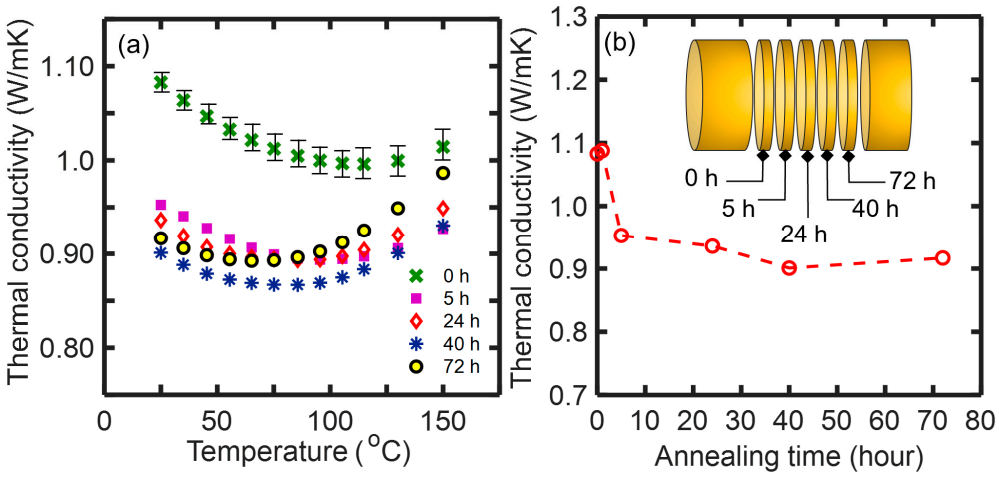

Figure 4. Effect of annealing at 230 °C versus time on thermal conductivity of $(Bi_xSb_{1-x})_2Te_3$-5% glass nanocomposites (**a**) from 25 °C to 150 °C, and (**b**) at room temperature. The inset of (**b**) shows a schematic picture of the diced samples for annealing.

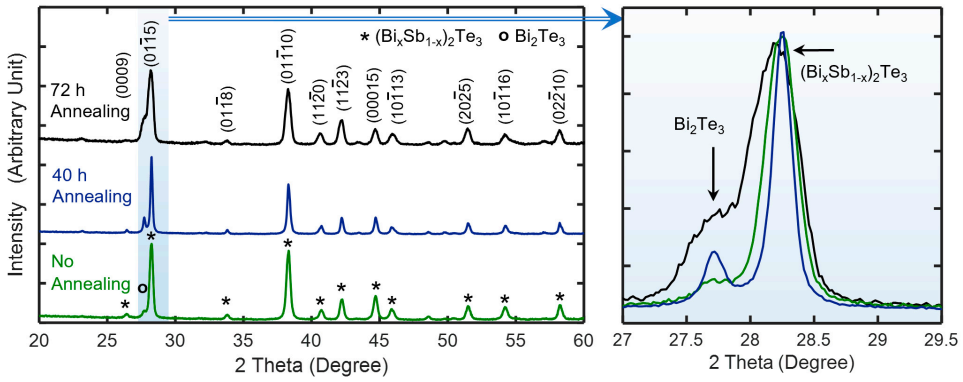

Figure 5. XRD patterns of the annealed $(Bi_xSb_{1-x})_2Te_3$-5% glass samples at 230 °C after 0, 40, and 72 h. The inset shows the comparison of the main peaks at 2θ = 27 to 29.5.

After optimizing the type of glass and annealing condition, $(Bi_{0.17}Sb_{0.83})_2Te_3$-5% glass was synthesized by SPS followed by MW processing and post-annealing. Table 2 lists the SPS, MW, and annealing conditions of the synthesized samples.

Table 2. Sintering parameters of microwave (MW) processed samples.

Sample ID	Composition	SPS Temp (°C)/Soak Time (min)	MW Temp (°C)	Second SPS Temp (°C)	Anneal Temp (°C)/Time (h)
SPS-MW-A0	$(Bi_{0.17}Sb_{0.83})_2Te_3$-5%Glass	540/1	500	400	-
SPS-MW-A3	$(Bi_{0.17}Sb_{0.83})_2Te_3$-5%Glass	540/1	500	400	230/3
SPS-MW-A40	$(Bi_{0.17}Sb_{0.83})_2Te_3$-5%Glass	540/1	500	400	230/40

Figure 6a shows that the electrical conductivity of MW-processed samples reduces by annealing time at 230 °C. Reduction in the electrical conductivity of samples with temperature is because of the bipolar effect at high temperature that electron–phonon scattering decreases carrier mobility. In the $(Bi_xSb_{1-x})_2Te_3$ alloy system, the electrical conductivity increases by decreasing x. However, the electrical conductivity of SPS-MW-A0 is less than crystalline and nanostructured alloys with larger x (x = 0.2) [2]. This is probably due to the crystal defects that are induced by MW processing as well as glass inclusions that decrease the mobility. Annealing can change the carrier concentration of MW-processed samples by adjusting the concentration of defects. Figure 6b shows that the Seebeck coefficient increases by annealing time. Lower electrical conductivity and higher Seebeck coefficient of SPS-MW-A40 indicate that the carrier concentration is compensated by annealing. The Seebeck coefficient is improved by 20% after 40 h of annealing. Annealing also improves the low-temperature PF and reduces the high-temperature PF (Figure 6c). The PF of SPS-MW-A40 is ~32 μW/cmK^2 at room temperature.

The thermal conductivity of the samples was strongly affected by annealing time (Figure 6d), wherein the thermal conductivity of the samples decreased in all temperature ranges, in particular, the thermal conductivity reduced from 0.91 W/mK to 0.77 W/mK at room temperature. This is one of the lowest thermal conductivity values with this range of zT reported for $(Bi_{0.17}Sb_{0.83})_2Te_3$ alloy at room temperature. The reduced thermal conductivity is owing to the addition of glass inclusions, development of a composite structure as a result of MW radiation, migration of defects, and stress relaxation. Annealing of the samples reduces the electronic portion of the thermal conductivity by compensating the dopant level. Annealing of the MW-processed samples increases the PF and reduces the thermal conductivity, simultaneously.

Figure 6e demonstrates temperature-dependent zT of the nanocomposite $(Bi_{0.17}Sb_{0.83})_2Te_3$-5% glass samples. An increase in PF, along with a significant reduction in thermal conductivity of SPS-MW-A40, resulted in considerable improvement in zT (=1.2) at room temperature. Therefore, annealing has a critical effect on optimizing TE properties of MW-processed $(Bi_xSb_{1-x})_2Te_3$ nanocomposites

with glass inclusions. Compared to conventional TE materials, SPS-MW-A40 sample demonstrated ~50% reduction in thermal conductivity and 33% improvement in zT at room temperature while maintaining a similar Seebeck coefficient that enables the application of this material as wearable power generators and coolers where high contact resistance is involved [39]. In comparison to the state-of-the-art $(Bi_xSb_{1-x})_2Te_3$ alloys wherein maximum TE properties were obtained at above 100 °C [2,6], MW processing helped to achieve the best performance of these alloys at room temperature. Therefore, these materials are optimum for room temperature applications.

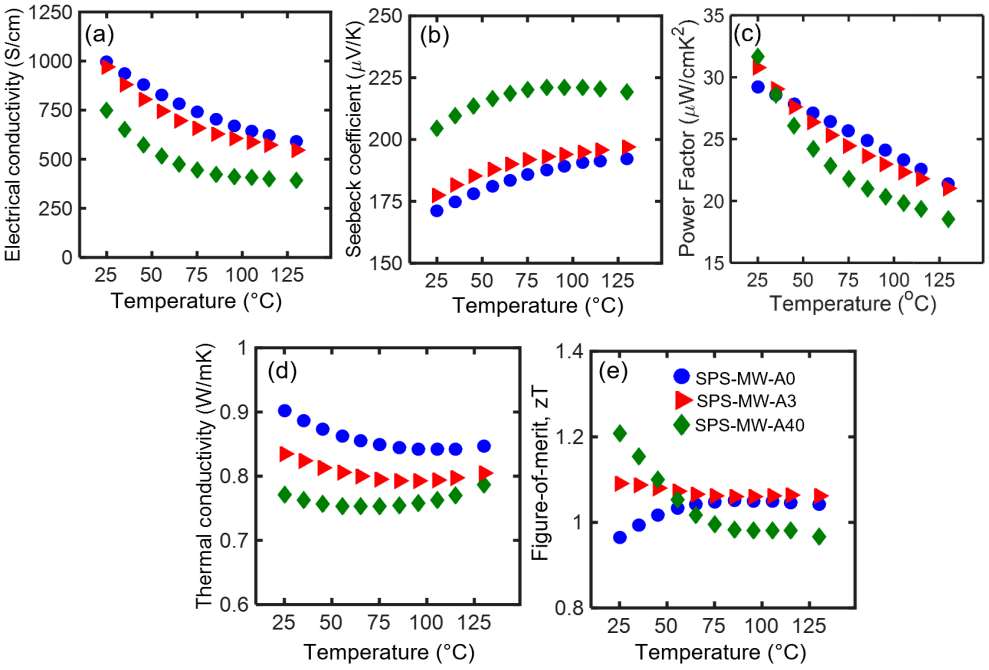

Figure 6. Comparison of (**a**) electrical conductivity, (**b**) Seebeck coefficient, (**c**) PF, (**d**) thermal conductivity, and (**e**) zT of spark plasma sintering (SPS)-MW-A0, SPS-MW-A3, and SPS-MW-A40 samples. The sample names are defined in Table 2.

Figure 7 represents backscattered SEM images of a cleaved surface of SPS-MW-A40 in two different magnifications. Backscattered electrons are applied to characterize phase contrast between areas with dissimilar chemical composition. Atoms with high atomic numbers backscatter electrons stronger than small atomic number atoms. Therefore, regions with high atomic number atoms look brighter [40]. In Figure 7a, brighter regions are the Bi-rich phase. A higher magnification image (Figure 7b) of SPS-MW-A40 shows a layered $(Bi_xSb_{1-x})_2Te_3$ structure with uniformly dispersed glass inclusions (dark particles). The $(Bi_xSb_{1-x})_2Te_3$ matrix has a layered structure in which the thickness of each layer is in the range of ~100 nm.

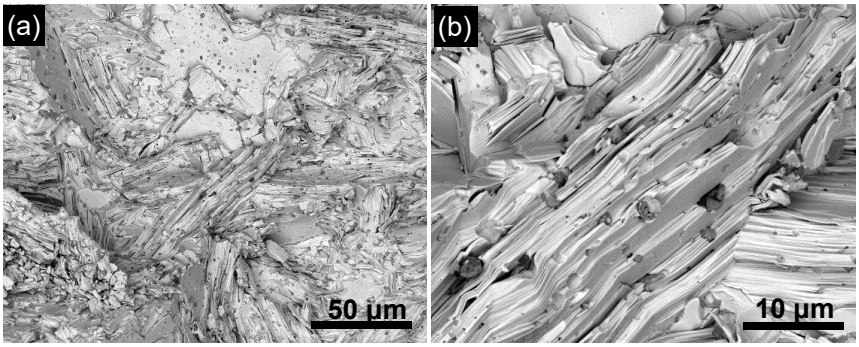

Figure 7. (**a**,**b**) SEM images of SPS-MW-A40 at different magnifications showing the dispersion of glass inclusions.

The optimized p-type $(Bi_{0.17}Sb_{0.83})_2Te_3$-5% glass nanocomposite and commercial n-type material were used to fabricate a thermoelectric generator (TEG) for a body heat harvesting application (Figure 8a). The details of a similar device fabrication process are explained elsewhere [39]. Figure 8b shows a body heat harvester wristband device made from the developed TEG, a heat spreader connected to body skin, a heatsink on the cold side for efficient heat rejection from the TEG, and a DC–DC boost converter connected to an LED lamp. As soon as the wristband touches the body's skin, the LED turns on, and it remains on as long the device is in contact with body skin. This device generates up to 300 µW power. Figure 8c,d compares the commercial TEG (from Marlow Industries) with the developed TEG in this study with the same size and conditions. Compared to the commercial TEG that generates 41 mV, our TEG made of optimized nanocomposite $(Bi_xSb_{1-x})_2Te_3$ alloy produces 323 mV. This outstanding achievement enables the usage of TEGs to power future wearable electronic devices.

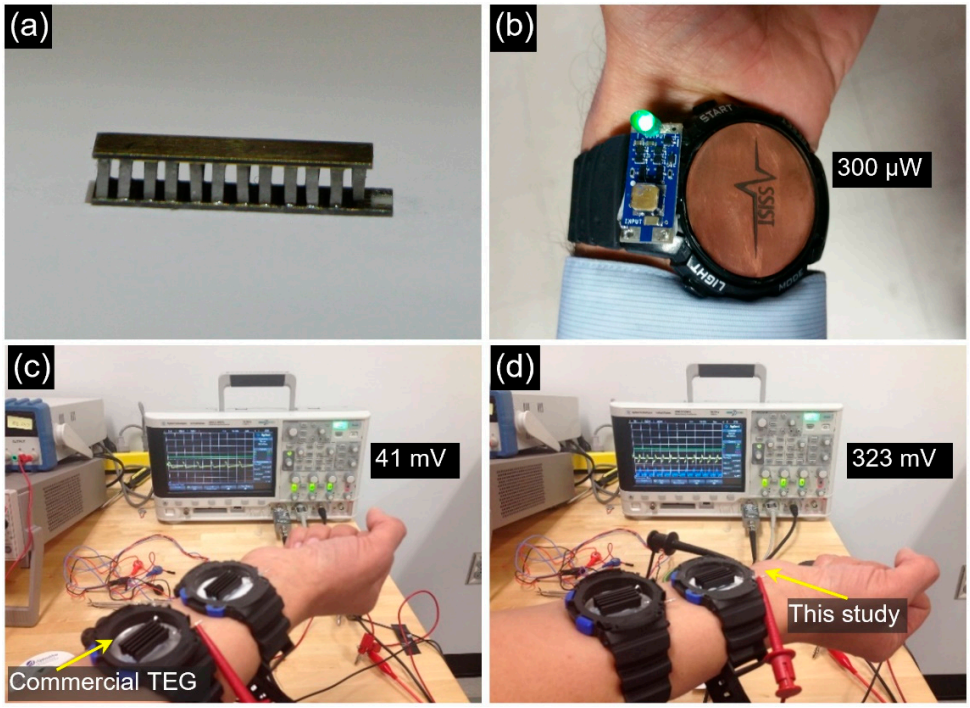

Figure 8. (**a**) Thermoelectric generator (TEG) module made from developed p-type $(Bi_xSb_{1-x})_2Te_3$ nanocomposite and commercial n-type material. (**b**) A complete device powering an LED using body heat. (**c**,**d**) Comparison of the commercial and the TEG developed in this study on a wristband in a similar condition.

4. Conclusions

High-performance p-type $(Bi_xSb_{1-x})_2Te_3$ nanocomposites with optimum properties at room temperature were synthesized for wearable devices. The effect of microwave processing, the addition of glass inclusion, and annealing was investigated to shift the optimum thermoelectric properties of $(Bi_xSb_{1-x})_2Te_3$ alloys to room temperature. Different glasses were tested, and it was found that 5% EG2964 Ferro glass (made of Bi, Zn, and B) provides optimum properties at room temperature. The addition of glass resulted in Seebeck coefficient improvement. Microwave processing, followed by annealing, enables controlling of the defect and carrier concentration levels. Annealing helped to minimize thermal conductivity. A zT of 1.2 along with lower thermal conductivity and higher Seebeck coefficient at room temperature was achieved in the microwave processed $(Bi_{0.17}Sb_{0.83})_2Te_3$-5% glass sample followed by annealing at 230 °C. The thermoelectric generator device made of these optimized materials provided 300 µW power on a body wearable platform. This study introduces microwave processing as a new and effective method of synthesizing high-performance p-type $(Bi_xSb_{1-x})_2Te_3$ alloys.

Author Contributions: A.N. and D.V. conceived the idea. A.N. and D.V. performed the experiments. D.V. supervised the research. A.N. and D.V. contributed to writing the paper and discussions. All authors have read and agreed to the published version of the manuscript.

Funding: This study is partially based upon work supported by the Air Force Office of Scientific Research (AFOSR) under contract number FA9550-19-1-0363 and the National Science Foundation (NSF) under grant numbers ECCS-1351533, ECCS-1515005, and ECCS-1711253.

Acknowledgments: This work was performed in part at the Analytical Instrumentation Facility (AIF) at North Carolina State University, which is supported by the State of North Carolina and the National Science Foundation (award number ECCS-1542015). The AIF is a member of the North Carolina Research Triangle Nanotechnology Network (RTNN), a site in the National Nanotechnology Coordinated Infrastructure (NNCI).

Conflicts of Interest: The authors declare no conflict of interest.

References

1. Vining, C.B. *Thermoelectric Properties of Silicides, CRC Handbook of Thermoelectrics*; CRC Press: Boca Raton, FL, USA, 1995; pp. 277–286.
2. Poudel, B.; Hao, Q.; Ma, Y.; Lan, Y.; Minnich, A.; Yu, B.; Yan, X.; Wang, D.; Muto, A.; Vashaee, D.; et al. High-thermoelectric performance of nanostructured bismuth antimony telluride bulk alloys. *Science* **2008**, *320*, 634–638. [CrossRef] [PubMed]
3. Xie, W.; Tang, X.; Yan, Y.; Zhang, Q.; Tritt, T.M. Unique nanostructures and enhanced thermoelectric performance of melt-spun BiSbTe alloys. *Appl. Phys. Lett.* **2009**, *94*, 102111. [CrossRef]
4. Fan, S.; Zhao, J.; Guo, J.; Yan, Q.; Ma, J.; Hng, H.H. p-type $Bi_{0.4}Sb_{1.6}Te_3$ nanocomposites with enhanced figure of merit. *Appl. Phys. Lett.* **2010**, *96*, 182104. [CrossRef]
5. Mehta, R.J.; Zhang, Y.; Karthik, C.; Singh, B.; Siegel, R.W.; Tasciuc, T.B.; Ramanath, G. A new class of doped nanobulk high-figure-of-merit thermoelectrics by scalable bottom-up assembly. *Nat. Mater.* **2012**, *11*, 233–240. [CrossRef]
6. Kim, S.I.; Lee, K.H.; Mun, H.A.; Kim, H.S.; Hwang, S.W.; Roh, J.W.; Yang, D.J.; Shin, W.H.; Li, X.S.; Lee, Y.H.; et al. Dense dislocation arrays embedded in grain boundaries for high-performance bulk thermoelectrics. *Science* **2015**, *348*, 109–114. [CrossRef]
7. Dehkordi, A.M.; Vashaee, D. Enhancement in thermoelectric power factor of polycrystalline $Bi_{0.5}Sb_{1.5}Te_3$ by crystallite alignment. *Phys. Stat. Solidi* **2012**, *209*, 2131–2134.
8. Zide, J.M.O.; Vashaee, D.; Zeng, G.; Bowers, J.E.; Shakouri, A.; Gossard, A.C. Demonstration of electron filtering to increase the Seebeck coefficient in $In_{0.53}Ga_{0.47}As/In_{0.53}Ga_{0.28}Al_{0.19}$ As superlattices. *Phys. Rev. B* **2006**, *74*, 205335. [CrossRef]
9. Wang, X.W.; Lee, H.; Lan, Y.C.; Zhu, G.H.; Joshi, G.; Wang, D.Z.; Yang, J.; Muto, A.J.; Tang, M.Y.; Klatsky, J.S.; et al. Enhanced thermoelectric figure of merit in nanostructured n-type silicon germanium bulk alloy. *Appl. Phys. Lett.* **2008**, *93*, 193121. [CrossRef]
10. Bahk, J.H.; Bian, Z.; Zebarjadi, M.; Santhanam, P.; Ram, R.; Shakouri, A. Thermoelectric power factor enhancement by ionized nanoparticle scattering. *Appl. Phys. Lett.* **2011**, *99*, 072118. [CrossRef]
11. Mohebali, M.; Liu, Y.; Tayebi, L.; Krasinski, J.S.; Vashaee, D. Thermoelectric figure of merit of bulk $FeSi_2$–$Si_{0.8}Ge_{0.2}$ nanocomposite and a comparison with β-FeSi2. *Renew. Energy* **2015**, *74*, 940–947. [CrossRef]
12. Nozariasbmarz, A.; Roy, P.; Zamanipour, Z.; Dycus, J.H.; Cabral, M.J.; LeBeau, J.M.; Krasinski, J.S.; Vashaee, D. Comparison of thermoelectric properties of nanostructured Mg_2Si, $FeSi_2$, SiGe, and nanocomposites of SiGe–Mg_2Si, SiGe–$FeSi_2$. *APL Mater.* **2016**, *4*, 104814. [CrossRef]
13. Nozariasbmarz, A.; Agarwal, A.; Coutant, Z.A.; Hall, M.J.; Liu, J.; Liu, R.; Malhotra, A.; Norouzzadeh, P.; Ramesh, V.P.; Sargolzaeiaval, Y.; et al. Thermoelectric silicides: A review. *Vashaee Jpn. J. Appl. Phys.* **2017**, *56*, 05DA04. [CrossRef]
14. Satyala, N.; Norouzzadeh, P.; Vashaee, D. Nano Bulk Thermoelectrics: Concepts, Techniques, and Modeling. In *Thermoelectrics Nanoscale*; Springer: Cham, Switzerland, 2014; pp. 141–183.
15. Misra, V.; Bozkurt, A.; Calhoun, B.; Jackson, T.; Jur, J.S.; Lach, J.; Lee, B.; Muth, J.; Oralkan, Ö.; Öztürk, M.; et al. Flexible technologies for self-powered wearable health and environmental sensing. *Proc. IEEE* **2015**, *103*, 661–685. [CrossRef]
16. Suarez, F.; Nozariasbmarz, A.; Vashaee, D.; Öztürk, M.C. Designing thermoelectric generators for self-powered wearable electronics. *Energy Environ. Sci.* **2016**, *9*, 2099–2113. [CrossRef]

17. Kishore, R.A.; Nozariasbmarz, A.; Poudel, B.; Sanghadasa, M.; Priya, S. Ultra-high performance wearable thermoelectric coolers with less materials. *Nat. Commun.* **2019**, *10*, 1765. [CrossRef] [PubMed]
18. Nozariasbmarz, A.; Collins, H.; Dsouza, K.; Polash, M.H.; Hosseini, M.; Hyland, M.; Liu, J.; Malhotra, A.; Mohaddes, F.; Ortiz, F.M.; et al. Review of wearable thermoelectric energy harvesting: From body temperature to electronic systems. *Appl. Energy* **2020**, *258*, 114069. [CrossRef]
19. Vineis, C.J.; Shakouri, A.; Majumdar, A.; Kanatzidis, M.G. Nanostructured thermoelectrics: Big efficiency gains from small features. *Adv. Mater.* **2010**, *22*, 3970–3980. [CrossRef]
20. Venkatasubramanian, R.; Siivola, E.; Colpitts, T.; O'Quinn, B. Thin-film thermoelectric devices with high room-temperature figures of merit. *Nature* **2001**, *413*, 597–602. [CrossRef]
21. Vashaee, D.; Nozariasbmarz, A.; Tayebi, L.; Krasinski, J.S. Microwave Processing of Thermoelectric Materials and Use of Glass Inclusions for Improving the Mechanical and Thermoelectric Properties. U.S. Patent App. 15/778,704; International Application No.: PCT/US2016/064292, 6 December 2018.
22. Nozariasbmarz, A.; Dsouza, K.; Vashaee, D. Field induced decrystallization of silicon: Evidence of a microwave non-thermal effect. *Appl. Phys. Lett.* **2018**, *112*, 093103. [CrossRef]
23. Nozariasbmarz, A. In-Situ Sintering Decrystallization of Thermoelectric Materials Using Microwave Radiation. Ph.D. Thesis, North Carolina State University, Raleigh, NC, USA, 2017.
24. Cheng, J.; Agrawal, D.; Zhang, Y.; Roy, R.; Santra, A.K. Synthesis of amorphous Si–Ge alloys using microwave energy. *J. Alloys Comp.* **2010**, *491*, 517–521. [CrossRef]
25. Nozariasbmarz, A.; Krasinski, J.S.; Vashaee, D. N-Type Bismuth Telluride Nanocomposite Materials Optimization for Thermoelectric Generators in Wearable Applications. *Materials* **2019**, *12*, 1529. [CrossRef]
26. Peelamedu, R.; Roy, R.; Agrawal, D.; Drawl, W.J. Field decrystallization and structural modifications of highly doped silicon in a 2.45-GHz microwave single-mode cavity. *Mater. Res.* **2004**, *19*, 1599–1602. [CrossRef]
27. Savary, E.; Gascoin, F.; Marinel, S. Fast synthesis of nanocrystalline Mg2Si by microwave heating: A new route to nano-structured thermoelectric materials. *Dalton Trans.* **2010**, *39*, 11074–11080. [CrossRef] [PubMed]
28. Shu-cai, Z.; Chen-guang, B. Microwave direct synthesis and thermoelectric properties of Mg_2Si by solid-state reaction. *Trans. Nonferrous Met. Soc. China* **2011**, *21*, 1785–1789. [CrossRef]
29. Kim-Hak, O.; Soulier, M.; Szkutnik, P.D.; Saunier, S.; Simon, J.; Goeuriota, D. Microwave sintering and thermoelectric properties of p-type $(Bi_{0.2}Sb_{0.8})_2Te_3$ powder. *Powder Technol.* **2012**, *226*, 231–234. [CrossRef]
30. Fan, X.A.; Yang, Y.; Xie, Z.; Li, K.; Zhu, W.; Duan, X.K.; Xiao, C.J.; Zhang, Q.Q. Bi2Te3 hexagonal nanoplates and thermoelectric properties of n-type Bi_2Te_3 nanocomposites. *J. Phys. D Appl. Phys.* **2007**, *40*, 5975. [CrossRef]
31. FERRO. Available online: https://www.ferro.com/-/media/files/resources/electronic-materials/ferro-electronic-materials-low-temperature-lead-free-glass-powders.pdf (accessed on 27 August 2020).
32. FERRO. Available online: https://www.yumpu.com/en/document/read/20793750/low-temperature-pb-free-glasses-ferro (accessed on 27 August 2020).
33. Kishore, R.A.; Nozariasbmarz, A.; Poudel, B.; Priya, S. High-Performance Thermoelectric Generators for Field Deployments. *ACS Appl. Mater. Interfaces* **2020**, *12*, 10389–10401. [CrossRef]
34. Nozariasbmarz, A.; Kishore, R.A.; Poudel, B.; Saparamadu, U.; Li, W.; Cruz, R.; Priya, S. High Power Density Body Heat Energy Harvesting. *ACS Appl. Mater. Interfaces* **2019**, *11*, 40107–40113. [CrossRef]
35. Satyala, N.; Krasinski, J.S.; Vashaee, D. Simultaneous enhancement of mechanical and thermoelectric properties of polycrystalline magnesium silicide with conductive glass inclusion. *Acta Mater.* **2014**, *74*, 141–150. [CrossRef]
36. FERRO. Available online: https://www.ferro.com/products/product-category/electronic-materials (accessed on 27 August 2020).
37. Roy, R.; Peelamedu, R.; Hurtt, L.; Agrawal, J.C.D. Definitive experimental evidence for Microwave Effects: Radically new effects of separated E and H fields, such as decrystallization of oxides in seconds. *Mater. Res. Innov.* **2002**, *6*, 128–140. [CrossRef]
38. Nozariasbmarz, A.; Hosseini, M.; Vashaee, D. Interfacial ponderomotive force in solids leads to field induced dissolution of materials and formation of non-equilibrium nanocomposites. *Acta Mater.* **2019**, *179*, 85–92. [CrossRef]

39. Nozariasbmarz, A.; Suarez, F.; Dycus, J.H.; Cabral, M.J.; LeBeau, J.M.; Öztürk, M.C.; Vashaee, D. Thermoelectric generators for wearable body heat harvesting: Material and device concurrent optimization. *Nano Energy* **2020**, *67*, 104265. [CrossRef]
40. Goldstein, J.; Newbury, D.E.; Joy, D.C.; Lyman, C.E.; Echlin, P.; Lifshin, E.; Sawyer, L.; Michael, J.R. *Scanning Electron Microscopy and X-ray Microanalysis*, 3rd ed.; Springer: New York, NY, USA, 2003.